Centrum voor Wiskunde en Informatica
Centre for Mathematics and Computer Science

P.W. Hemker, B. Koren

Multigrid, defect correction and upwind schemes
for the steady Navier-Stokes equations

Department of Numerical Mathematics Note NM-N8802 February

The Centre for Mathematics and Computer Science is a research institute of the Stichting Mathematisch Centrum, which was founded on February 11, 1946, as a nonprofit institution aiming at the promotion of mathematics, computer science, and their applications. It is sponsored by the Dutch Government through the Netherlands Organization for the Advancement of Pure Research (Z.W.O.).

Multigrid, Defect Correction and Upwind Schemes for the Steady Navier-Stokes Equations

P.W. Hemker, B. Koren
Centre for Mathematics and Computer Science
P.O. Box 4079, 1009 AB Amsterdam, The Netherlands

A computational method for the full, steady, 2D, compressible Navier-Stokes equations is evaluated. The method is hybrid in the sense that it can be used equally well for the steady Euler equations. An upwind finite volume technique is applied for the discretization of the convective terms in the Navier-Stokes equations. For the diffusive terms, a central finite volume technique is applied. As a basic scheme to solve the nonlinear system of discretized equations, symmetric point Gauss-Seidel relaxation is used. Herein, one or more Newton steps are used for the collective relaxation of the four unknowns in each finite volume. Nonlinear multigrid is applied as an acceleration technique. The process is started by nested iteration. The difficulty in inverting a higher-order accurate operator is by-passed by using defect correction as an outer iteration for the nonlinear multigrid cycling. Computational results are presented for a sub- and supersonic flat plate flow, the latter with an oblique shock wave impinging on the boundary layer. The multigrid technique appears to be efficient and reliable results are obtained.

1980 Mathematics Subject Classification: 65B05, 65N05, 65N10, 65N20, 65N30, 76N05, 76N10.
Key Words and Phrases: convection diffusion equations, upwind schemes, multigrid methods, defect correction.
Note: This work was supported by the European Space Agency (ESA), via Avions Marcel Dassault - Bréguet Aviation (AMD-BA). It has been presented at the HERMES Hypersonic Research Program Meeting, November 23-25, 1987, Stuttgart. The present report is a synopsis of two detailed reports which are to appear [9, 10].

1. Introduction

Mainly based on existing computational methods for the Euler equations, several Navier-Stokes methods have been developed recently [1, 16, 17, 20]. Based on our Euler method [4, 6, 7, 8, 11, 18, 19] we followed the same approach [9, 10]. Our first objective was the efficient and accurate computation of laminar, steady, 2D, compressible flows at practically relevant (i.e. high) Reynolds numbers, but (still) subsonic or low-supersonic Mach numbers. The non-isenthalpic Euler code developed earlier appeared to be a good starting point for this purpose.

2. Flow model

The Navier-Stokes equations considered are

$$\frac{\partial f(q)}{\partial x} + \frac{\partial g(q)}{\partial y} - \frac{1}{Re}\left\{\frac{\partial r(q)}{\partial x} + \frac{\partial s(q)}{\partial y}\right\} = 0, \tag{2.1}$$

with $f(q)$ and $g(q)$ the convective flux vectors, Re the Reynolds number, and $r(q)$ and $s(q)$ the diffusive flux vectors. As state vector q we consider the conservative vector $q = (\rho, \rho u, \rho v, \rho e)$, with for the total energy e the perfect gas relation $e = p/(\rho(\gamma-1)) + \frac{1}{2}(u^2+v^2)$. The primitive quantities used so far are: the ratio of specific heats γ, density ρ, pressure p and the velocity components u and v. The quantity γ is assumed to be constant. The convective flux vectors are defined by

$$f(q) = \begin{bmatrix} \rho u \\ \rho u^2 + p \\ \rho uv \\ \rho u(e + p/\rho) \end{bmatrix}, \quad g(q) = \begin{bmatrix} \rho v \\ \rho uv \\ \rho v^2 + p \\ \rho v(e + p/\rho) \end{bmatrix}, \text{ and} \tag{2.2}$$

the diffusive flux vectors by

$$r(q) = \begin{bmatrix} 0 \\ \tau_{xx} \\ \tau_{xy} \\ \tau_{xx}u + \tau_{xy}v + \dfrac{1}{\gamma-1}\dfrac{1}{Pr}\dfrac{\partial(c^2)}{\partial x} \end{bmatrix}, \quad s(q) = \begin{bmatrix} 0 \\ \tau_{xy} \\ \tau_{yy} \\ \tau_{yy}v + \tau_{xy}u + \dfrac{1}{\gamma-1}\dfrac{1}{Pr}\dfrac{\partial(c^2)}{\partial y} \end{bmatrix}, \tag{2.3}$$

Note NM-N8802
Centre for Mathematics and Computer Science
P.O. Box 4079, 1009 AB Amsterdam, The Netherlands

with Pr the Prandtl number, c the speed of sound (for a perfect gas $c = \sqrt{\gamma p/\rho}$), and with τ_{xx}, τ_{xy} and τ_{yy} the viscous stresses. Assuming the diffusion coefficients to be constant and Stokes' hypothesis to hold, the stresses are written as

$$\tau_{xx} = \frac{4}{3}\frac{\partial u}{\partial x} - \frac{2}{3}\frac{\partial v}{\partial y}, \tag{2.4a}$$

$$\tau_{xy} = \frac{\partial u}{\partial y} + \frac{\partial v}{\partial x}, \tag{2.4b}$$

$$\tau_{yy} = \frac{4}{3}\frac{\partial v}{\partial y} - \frac{2}{3}\frac{\partial u}{\partial x}. \tag{2.4c}$$

3. Discretization method

To still allow Euler flow ($1/Re = 0$) solutions with discontinuities, the equations are discretized in the integral form. A straightforward and simple discretization of the integral form is obtained by subdividing the integration region Ω into quadrilateral finite volumes $\Omega_{i,j}$, and by requiring that the conservation laws hold for each finite volume separately:

$$\int_{\partial\Omega_{i,j}} (f(q)n_x + g(q)n_y)ds - \frac{1}{Re}\int_{\partial\Omega_{i,j}} (r(q)n_x + s(q)n_y)ds = 0, \quad \forall i,j. \tag{3.1}$$

For the evaluation of the convective flux vectors we make use of the rotational invariance of the Navier-Stokes equations. We do not do so for the diffusive flux vectors. Given our simple central discretization of diffusive terms, use of rotational invariance for the latter is hardly advantageous. Thus, the discretized equations become

$$\int_{\partial\Omega_{i,j}} T^{-1}(n_x,n_y)f(T(n_x,n_y)q)ds - \frac{1}{Re}\int_{\partial\Omega_{i,j}} (r(q)n_x + s(q)n_y)ds = 0, \quad \forall i,j, \tag{3.2}$$

with $T(n_x,n_y)$ the rotation matrix

$$T = \begin{bmatrix} 1 & 0 & 0 & 0 \\ 0 & n_x & n_y & 0 \\ 0 & -n_y & n_x & 0 \\ 0 & 0 & 0 & 1 \end{bmatrix}. \tag{3.3}$$

3.1 Evaluation of convective fluxes

For convection dominated flows, our objective, a proper evaluation of the convective flux vectors is of paramount importance. Based on previous experience, for this we prefer an upwind approach. Following the Godunov principle, along each finite volume wall we assume the convective flux vector to be constant, and to be determined by a constant left and right state only.

3.1.1. Approximation of left and right state. The approximation of the left and right state determines the accuracy of the convective discretization. First- and higher-order accurate discretizations can be made [4]. Considering for instance the numerical flux function $(f(q))_{i+\frac{1}{2},j} = f(q^l_{i+\frac{1}{2},j}, q^r_{i+\frac{1}{2},j})$, where the superscripts l and r refer to the left and right side of volume wall $\partial\Omega_{i+\frac{1}{2},j}$ (Fig. 3.1), first-order accuracy is obtained by taking

$$q^l_{i+\frac{1}{2},j} = q_{i,j}, \text{ and} \tag{3.4a}$$

$$q^r_{i+\frac{1}{2},j} = q_{i+1,j}. \tag{3.4b}$$

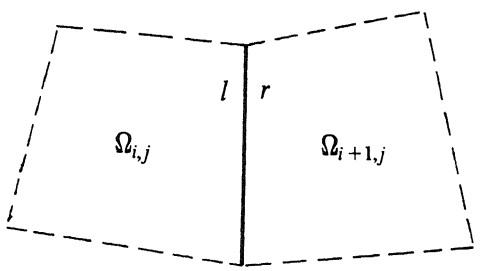

Fig. 3.1. Volume wall $\partial\Omega_{i+\frac{1}{2},j}$.

Higher-order accuracy can simply be obtained with the κ-schemes as introduced by van Leer [13]:

$$q^l_{i+\frac{1}{2},j} = q_{i,j} + \frac{1+\kappa}{4}(q_{i+1,j} - q_{i,j}) + \frac{1-\kappa}{4}(q_{i,j} - q_{i-1,j}), \text{ and} \tag{3.5a}$$

$$q^r_{i+\frac{1}{2},j} = q_{i+1,j} + \frac{1+\kappa}{4}(q_{i,j} - q_{i+1,j}) + \frac{1-\kappa}{4}(q_{i+1,j} - q_{i+2,j}), \tag{3.5b}$$

with $\kappa \in \mathbb{R}$ ranging from $\kappa = -1$ (fully one-sided upwind) to $\kappa = 1$ (central).
In [10] an optimal value for κ is found by giving an error analysis, using as model equation

$$\frac{\partial u}{\partial x} + \frac{\partial u}{\partial y} - \epsilon\left(\frac{\partial^2 u}{\partial x^2} + \frac{\partial^2 u}{\partial x \partial y} + \frac{\partial^2 u}{\partial y^2}\right) = 0. \tag{3.6}$$

On a grid with constant mesh size h, a finite volume discretization which uses the κ-approximation for the convective terms and which is second-order central for the diffusive terms, yields as modified equation

$$\begin{aligned}\frac{\partial u}{\partial x} + \frac{\partial u}{\partial y} - \epsilon\left(\frac{\partial^2 u}{\partial x^2} + \frac{\partial^2 u}{\partial x \partial y} + \frac{\partial^2 u}{\partial y^2}\right) + h^2 \frac{\kappa - 1/3}{4}\left(\frac{\partial^3 u}{\partial x^3} + \frac{\partial^3 u}{\partial y^3}\right) + \\ + h^3\left(\frac{\kappa - 1}{8} - \frac{1}{12}\frac{\epsilon}{h}\right)\left(\frac{\partial^4 u}{\partial x^4} + \frac{\partial^4 u}{\partial y^4}\right) + \\ + O(h^4) = 0.\end{aligned} \tag{3.7}$$

Assuming the reliability of the underlying Taylor series expansion, the modified equation clearly shows that the highest accuracy (third-order) is obtained for $\kappa = 1/3$ (upwind biased), and the lowest false diffusion for $\kappa = 1$ (central). Euler flow computations [8] have shown that for stability reasons the upwind biased approximation is to be preferred above the central approximation.
To avoid spurious non-monotonicity, a new limiter has been constructed for the $\kappa = 1/3$ approximation [10]. Let $q^{l(k)}_{i+\frac{1}{2},j}$ and $q^{r(k)}_{i+\frac{1}{2},j}$ be the *kth* component ($k = 1,2,3,4$) of $q^l_{i+\frac{1}{2},j}$ respectively $q^r_{i+\frac{1}{2},j}$. Then a limited left and right state can be written as

$$q^{l(k)}_{i+\frac{1}{2},j} = q^{(k)}_{i,j} + \frac{1}{2}\psi(R^{(k)}_{i,j})(q^{(k)}_{i,j} - q^{(k)}_{i-1,j}), \text{ and} \tag{3.8a}$$

$$q^{r(k)}_{i+\frac{1}{2},j} = q^{(k)}_{i,j} + \frac{1}{2}\psi(1/R^{(k)}_{i+1,j})(q^{(k)}_{i+1,j} - q^{(k)}_{i+2,j}), \tag{3.8b}$$

with $\psi(R)$ the limiter considered, and $R^{(k)}_{i,j}$ the ratio

$$R^{(k)}_{i,j} = \frac{q^{(k)}_{i+1,j} - q^{(k)}_{i,j}}{q^{(k)}_{i,j} - q^{(k)}_{i-1,j}}. \tag{3.9}$$

Using this notation, the limiter constructed for the $\kappa = 1/3$ approximation reads

$$\psi(R) = \frac{R + 2R^2}{2 - R + 2R^2}. \tag{3.10}$$

3.1.2. Solution of 1D Riemann problem. Osher's scheme [14] has been preferred so far for the approximate solution of the standard 1D Riemann problem thus obtained. Osher's scheme has been chosen because of: (i) its continuous differentiability, and (ii) its consistent treatment of boundary conditions. (The continuous differentiability guarantees the applicability of a Newton type solution technique, which is what we make use of.) The question arises whether it is still a good choice to use Osher's scheme when diffusion also has to be modelled. Another, more widespread upwind scheme used in Navier-Stokes codes is van Leer's flux splitting scheme [12, 16, 17, 20]. Reasons for its popularity are: (i) its likewise continuous differentiability, and (ii) its simplicity. The latter property is generally believed to be in contrast with Osher's scheme. (Recent work may help to reduce this difference, see e.g. [19].) In [9] a detailed error analysis is given for both schemes. The analysis is confined to the steady, 2D, isentropic Euler equations for a perfect mono-atomic gas:

$$\frac{\partial f(q)}{\partial x} + \frac{\partial g(q)}{\partial y} = 0, \quad \text{with} \tag{3.11}$$

$$f(q) = \begin{bmatrix} \rho u \\ \rho(u^2 + c^2) \\ \rho u v \end{bmatrix}, \quad g(q) = \begin{bmatrix} \rho v \\ \rho u v \\ \rho(v^2 + c^2) \end{bmatrix}. \tag{3.12}$$

(Notice that for an isentropic, perfect and mono-atomic gas c is a constant.) For a subsonic flow and a first-order accurate finite volume discretization on a grid with constant mesh size h, the system of modified equations has been derived for both Osher's and van Leer's scheme. For both systems we considered a subsonic shear flow (the new element) along a flat plate. For this Lamb's approximate solution was used. Substitution of Lamb's solution into the modified equation yields at the boundary layer edge a discretization error ratio as given in Fig. 3.2. In this figure, M_δ denotes the Mach number at the boundary layer edge. The analysis gives some evidence for the superiority of Osher's scheme above van Leer's scheme, when dealing with shear flows. In section 5 results will be presented which show this superiority for the Navier-Stokes equations indeed.

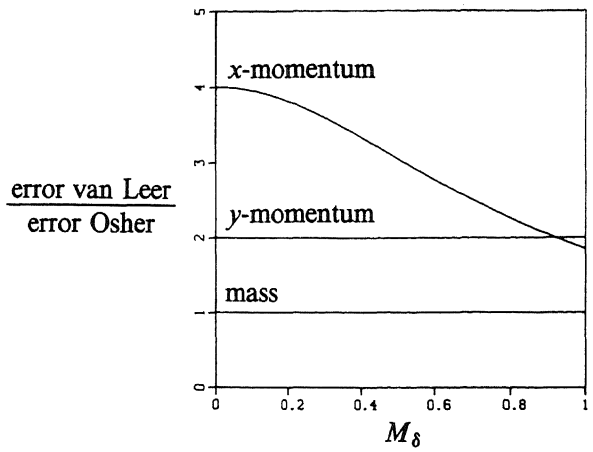

Fig. 3.2. Ratio of discretization errors at boundary layer edge.

3.2. Evaluation of diffusive fluxes

For the evaluation of the diffusive fluxes at a volume wall, it is necessary to compute grad(u), grad(v) and grad(c^2) at that wall. For this we use a standard technique [15]. To compute for instance $(\text{grad}(u))_{i+\frac{1}{2},j}$, we use Gauss' theorem:

$$(\nabla u)_{i+\frac{1}{2},j} = \frac{1}{A_{i+\frac{1}{2},j}} \int_{\partial\Omega_{i+\frac{1}{2},j}} u\,\underline{n}\,ds, \tag{3.13}$$

with $\partial\Omega_{i+\frac{1}{2},j}$ the boundary and $A_{i+\frac{1}{2},j}$ the area of a quadrilateral dummy volume $\Omega_{i+\frac{1}{2},j}$ (Fig. 3.3) of which the vertices $z=(x,y)$ are defined by:

$$z_{i,j\pm\frac{1}{2}} = \tfrac{1}{2}(z_{i-\frac{1}{2},j\pm\frac{1}{2}} + z_{i+\frac{1}{2},j\pm\frac{1}{2}}). \tag{3.14}$$

A similar expression exists for $z_{i\pm\frac{1}{2},j}$.

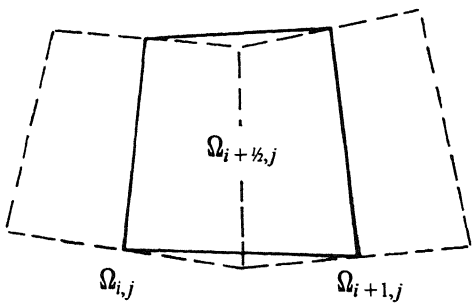

Fig. 3.3. Dummy volume $\Omega_{i+\frac{1}{2},j}$.

The line integrals $\int_{\partial\Omega_{i+\frac{1}{2},j}} un_x ds$ and $\int_{\partial\Omega_{i+\frac{1}{2},j}} un_y ds$ are approximated by

$$\begin{aligned}\int_{\partial\Omega_{i+\frac{1}{2},j}} u\,n_x\,ds = \quad & u_{i+1,j} \quad (y_{i+1,j+\frac{1}{2}} - y_{i+1,j-\frac{1}{2}}) \\ & + u_{i+\frac{1}{2},j+\frac{1}{2}} \quad (y_{i,j+\frac{1}{2}} - y_{i+1,j+\frac{1}{2}}) \\ & + u_{i,j} \quad (y_{i,j-\frac{1}{2}} - y_{i,j+\frac{1}{2}}) \\ & + u_{i+\frac{1}{2},j-\frac{1}{2}} \quad (y_{i+1,j-\frac{1}{2}} - y_{i,j-\frac{1}{2}}),\end{aligned} \tag{3.15a}$$

and

$$\begin{aligned}\int_{\partial\Omega_{i+\frac{1}{2},j}} u\,n_y\,ds = \quad & u_{i+1,j} \quad (x_{i+1,j-\frac{1}{2}} - x_{i+1,j+\frac{1}{2}}) \\ & + u_{i+\frac{1}{2},j+\frac{1}{2}} \quad (x_{i+1,j+\frac{1}{2}} - x_{i,j+\frac{1}{2}}) \\ & + u_{i,j} \quad (x_{i,j+\frac{1}{2}} - x_{i,j-\frac{1}{2}})\end{aligned} \tag{3.15b}$$

with for $u_{i+\frac{1}{2},j\pm\frac{1}{2}}$ the central expression

$$u_{i+\frac{1}{2},j\pm\frac{1}{2}} = \tfrac{1}{4}(u_{i,j} + u_{i,j\pm1} + u_{i+1,j} + u_{i+1,j\pm1}). \tag{3.16}$$

Similar expressions are used for the other gradients, and other walls. For sufficiently smooth grids this central diffusive flux computation is second-order accurate.

4. Solution method

To efficiently solve the system of discretized equations, symmetric point Gauss-Seidel relaxation, accelerated by nonlinear multigrid (FAS), is applied. With the scalar convection diffusion equation (3.6) as a model, local mode analysis shows that 'symmetric point Gauss-Seidel + multigrid' converges fast for the first-order discretized equation, for any value of the mesh Reynolds number h/ϵ [9]. However, it appears to converge very slowly for the higher-order ($\kappa=1/3$) discretized equation, for small and moderately large values of h/ϵ. It even appears to diverge for large values of h/ϵ [10]. The cause clearly is the higher-order discretization of the convection operator. No cure can be found in using some other $\kappa\in[-1,1]$ [10]. As with the Euler equations [4,8], the difficulty in inverting the higher-order operator is by-passed by introducing iterative defect correction (IDeC) as an outer iteration for the nonlinear multigrid cycling. Let $F_h(q_h)$ denote the full, higher-order accurate operator, and $\tilde{F}_h(q_h)$ the less accurate operator that can be easily inverted. Then iterative defect correction can be written as

$$\begin{aligned}&\tilde{F}_h(q_h^1) = 0, \\ &\tilde{F}_h(q_h^{n+1}) = \tilde{F}_h(q_h^n) - \omega F_h(q_h^n),\ n=1,2,\cdots,N,\end{aligned} \tag{4.1}$$

where n denotes the *nth* iterand, and ω a damping factor. The standard value for ω is: $\omega=1$. Special attention has been paid to the choice of the approximate operator $\tilde{F}_h(q_h)$ for the Navier-Stokes equations. The operator necessarily has only first-order accurate convection, but the amount of diffusion can be chosen freely. This freedom has been exploited by analyzing three approximate operators $\tilde{F}_h$: (i) an operator with full, second-order accurate diffusion, (ii) an operator with partial diffusion, and (iii) an operator without diffusion. The *first approximate operator* most closely resembles the higher-order operator F_h, and therefore has the best convergence properties. For sufficiently smooth problems and a second-order accurate F_h, for the first approximate operator, theory [2] predicts the solution to be second-order accurate after a single IDeC-cycle. Theory does not give this guarantee for the other approximate operators. The *second approximate operator* neglects the cross derivatives in the diffusive terms, but it has full second-order diffusion stemming from the remaining derivatives. The special feature of this operator is that for the evaluation of the convective and diffusive fluxes in the Navier-Stokes equations, the same five-point data structure can be used. The operator combines elegance and simplicity with a rather good resemblance to the higher-order operator. The *third approximate operator* considered was already known from the Euler work. Given its successful application there, it may be expected to be suitable for very large values of the mesh Reynolds number. Local mode analyses with (3.6) as a model equation, and experiments with the Navier-Stokes equations showed the first approximate operator to have the best convergence properties indeed. Its relative complexity has been taken for granted. The results presented in the next section have all been obtained with this operator. Though the mesh Reynolds numbers in the computations performed were large, we obeyed the rule $m_r+m_p>2m$ [2], where m_r and m_p denote the order of accuracy of the defect restriction and the correction prolongation respectively, and where $2m$ denotes the order of the differential equation(s) considered. We used a piecewise constant restriction ($m_r=1$) and a piecewise bilinear prolongation ($m_p=2$). For further details about the multigrid method applied we refer to [9].

5. Numerical results

To evaluate the computational method developed so far, the following flow problems have been considered: (i) a subsonic flat plate flow, and (ii) a supersonic flat plate flow with oblique shock wave - boundary layer interaction. For the subsonic problem, the Blasius solution is used as a reference. For the supersonic problem comparisons are made with experimental results obtained by Hakkinen et al. [3]. For both flow problems we used: $\gamma = 1.4$ and $Pr = 0.71$.

5.1. Subsonic flat plate flow

The geometry and boundary conditions for this flow problem are given in Fig. 5.1. As far as convection is concerned, the eastern boundary has been considered to be an outflow boundary. For diffusion the northern, southern and eastern boundary have been assumed to be far-field boundaries with zero diffusion. For this problem we only used grids composed of square finite volumes. As a coarsest grid in all multigrid computations we used: the 4×2-grid given in Fig. 5.2. For explicit details about boundary conditions and so on, we -again- refer to [9].

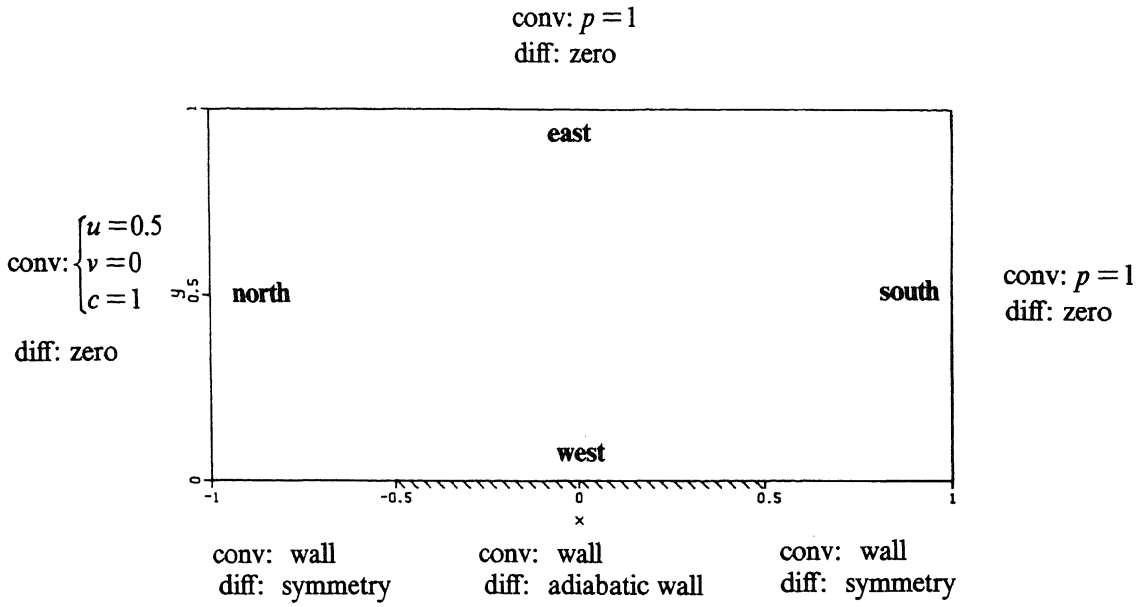

Fig. 5.1. Geometry and boundary conditions subsonic flat plate flow (conv: convection, diff: diffusion).

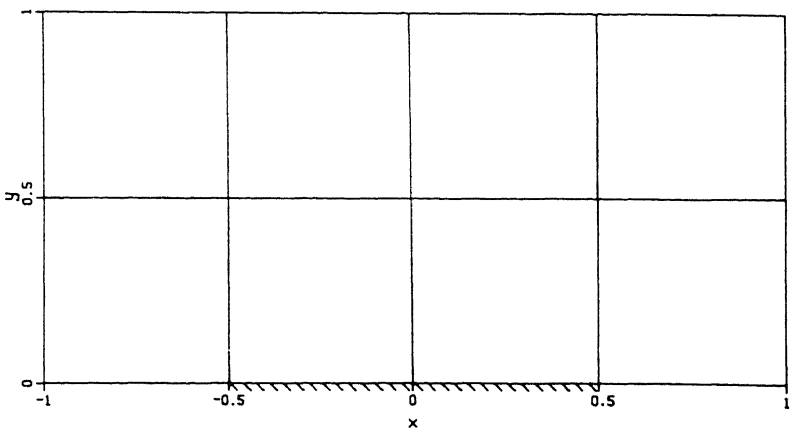

Fig. 5.2. Coarsest grid subsonic flat plate flow.

5.1.1. Osher's and van Leer's scheme. To compare Osher's and van Leer's scheme, we performed for both schemes an experiment with h- (mesh size) and Re-variation, using the first-order approximation only. (Because this will show best the differences). Results obtained are given in Fig. 5.3. The results clearly show the superiority of Osher's scheme, in particular under hard conditions (first-order approximation, high mesh Reynolds number). In further experiments, we continued with Osher's scheme only. (Notice that for both schemes the exact numerical solution has been obtained for $Re = 10^{100}$.)

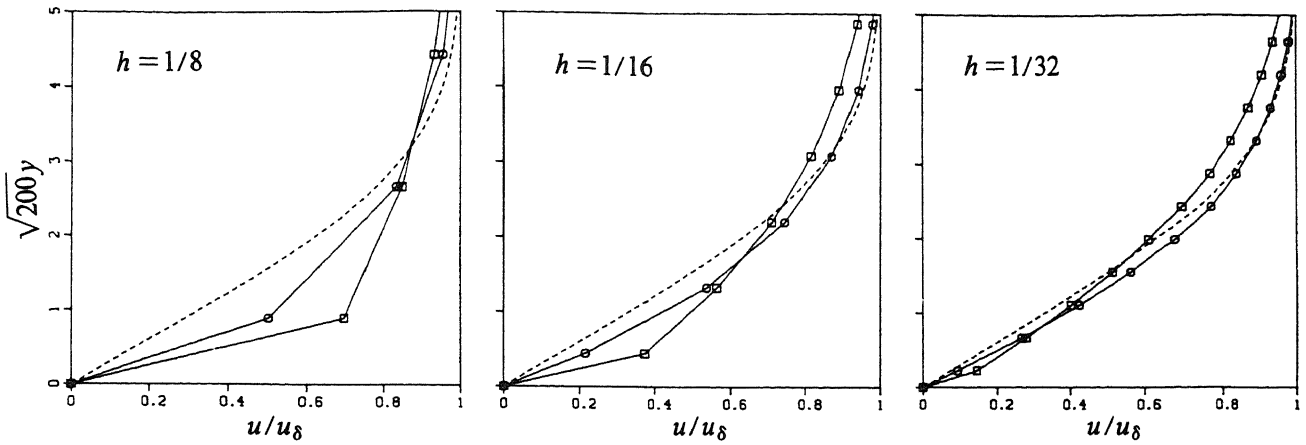

a. h-variation with $Re = 100$ (○ : Osher, □ : van Leer).

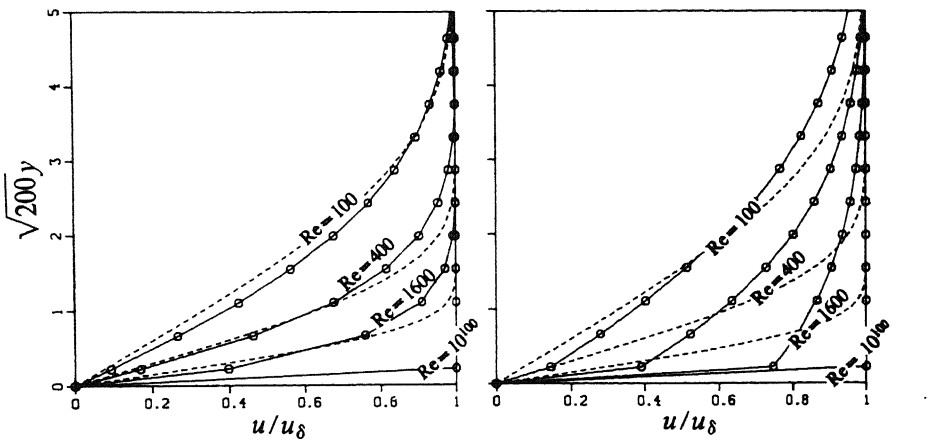

b. Re-variation with $h = 1/32$ (left: Osher, right: van Leer).

Fig. 5.3. Velocity profiles at $x = 0$ for the subsonic flat plate flow (-----: Blasius solution).

5.1.2. Multigrid behaviour. To investigate the convergence properties of the nonlinear multigrid technique we considered the subsonic flat plate flow at $Re = 100$, using the first-order discretized equations and Osher's approximate Riemann solver. Investigated have been: the measure of grid independence of the convergence rate, the multigrid effectiveness and the influence of the order of accuracy of the prolongation. To measure the grid independence, we performed 20 FAS-cycles on a 16×8-, a 32×16- and a 64×32-grid. For the multigrid effectiveness we performed 21 symmetric relaxation sweeps on the 64×32-grid. Further, to investigate the influence of the order of accuracy of the prolongation, we performed again 20 FAS-cycles with the 64×32-grid as finest grid, but now with the piecewise constant correction prolongation ($m_p = 1$, so violating the rule $m_r + m_p > 2m$). The results are found in Fig. 5.4. They clearly show that, for the flow considered, the multigrid method is nearly grid-independent and highly effective. The effect of the order of accuracy of the prolongation appears to be negligible.

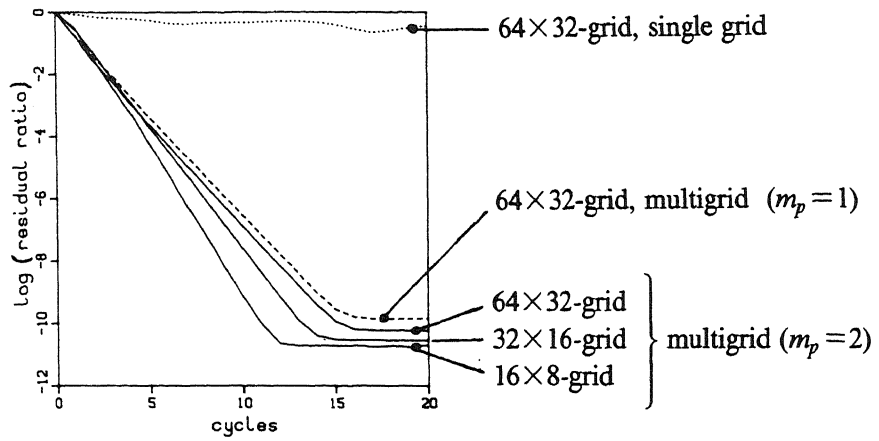

Fig. 5.4. Multigrid behaviour.

5.1.3. Convergence to first- and second-order accuracy. Theory predicts that a single FAS-cycle may be sufficient for obtaining first-order accuracy [4]. Further, as already mentioned, for smooth problems theory predicts a single IDeC-cycle to be sufficient for obtaining second-order accuracy [2]. To investigate the convergence properties with respect to these two predictions we computed again solutions on the 16×8-, 32×16- and 64×32-grid for $Re=100$. We performed the computations for successively the first-order and the (non-limited) $\kappa=1/3$ approximation. Solutions obtained after 1 FAS-cycle and 1 IDeC-cycle (with inside the latter only 1 FAS-cycle) are given in Fig. 5.5a respectively 5.5b. Assuming the Blasius solution to be the exact solution, it can be verified that the results obtained (more or less) satisfy the theoretical predictions. In order to compare, for both discretizations the fully converged solutions (square markers) have been given. Additionally, for the first-order discretization only, the single 64×32-grid solution as obtained after 1,2,3 and 4 symmetric relaxation sweeps has been given. The latter solutions clearly show once more the effectiveness of the multigrid technique.

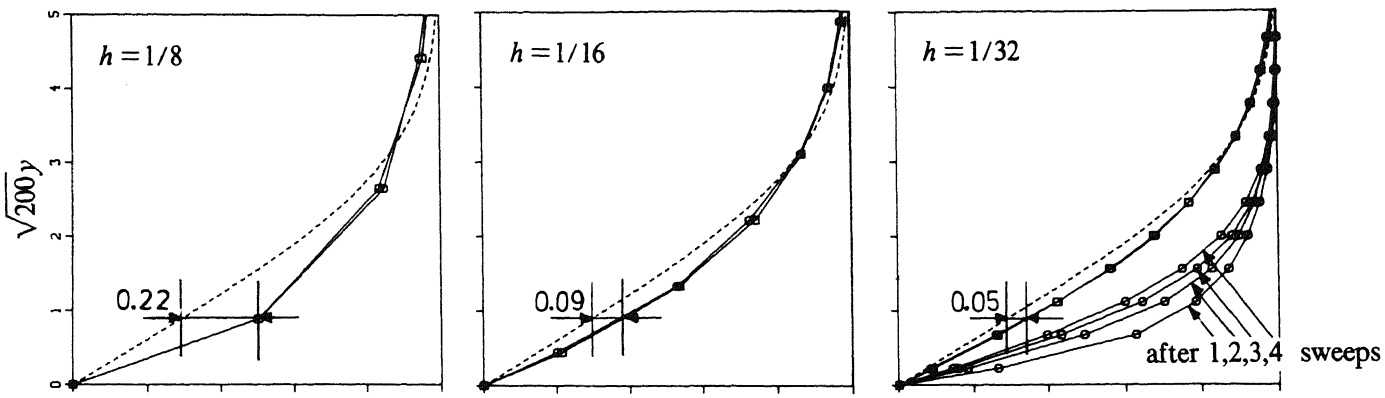

a. First-order (○ : after 1 FAS-cycle, □ : after 20 FAS-cycles).

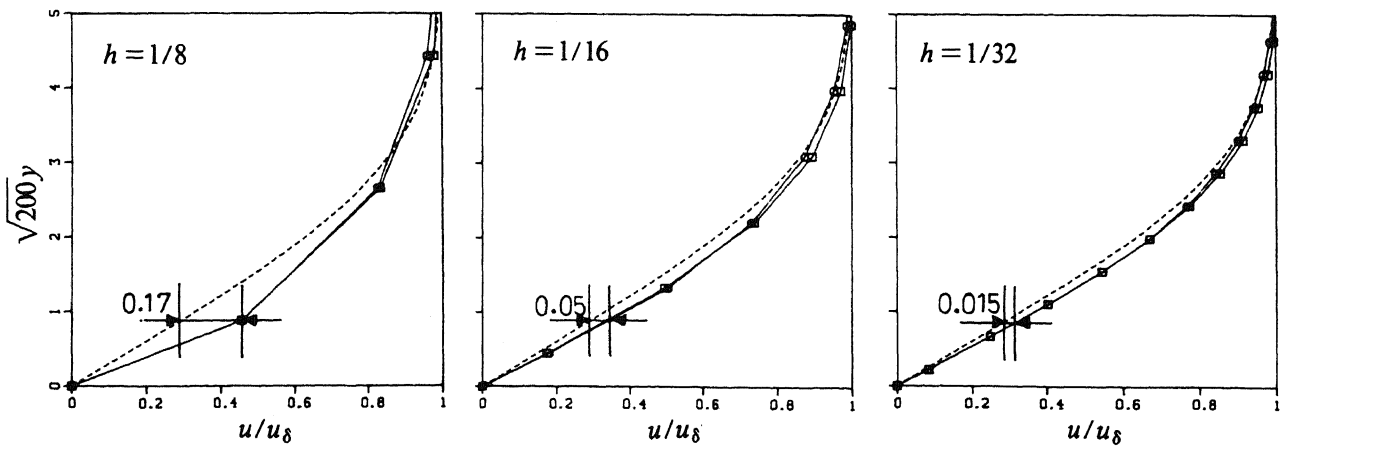

b. Non-limited second-order (○ : after 1 IDeC-cycle, □ : after 50 IDeC-cycles).

Fig. 5.5. Velocity profiles at $x=0$ for the subsonic flat plate flow (-----: Blasius solution).

5.2. Supersonic flat plate flow with oblique shock wave - boundary layer interaction

As reference test case from [3] we considered the experiment performed at $Re = 2.96\,10^5$. At first we tried to make a satisfactory grid. Since the present code has the possibility to compute Euler flows, it is easy to optimize the grid for convection only. For the present test case this led via the 80×32-grid shown in Fig.5.6a to the 80×32-grid in Fig. 5.6b.

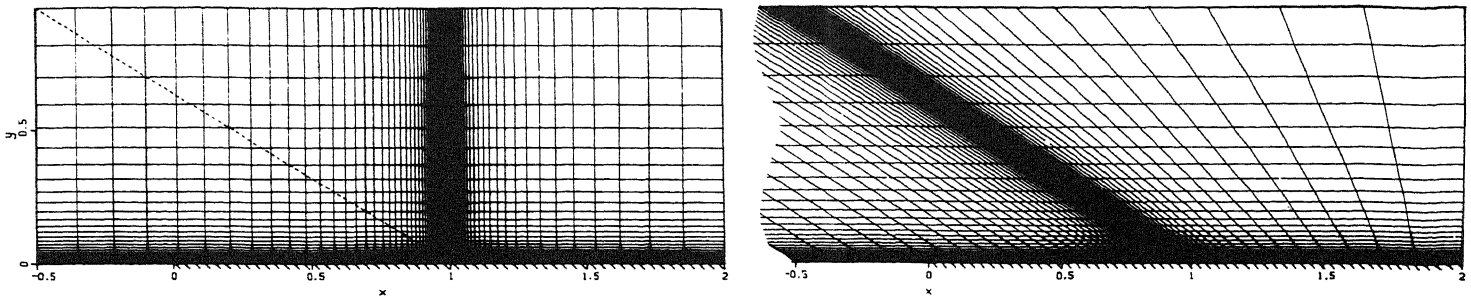

a. Rectangular grid (-----: shock wave). b. Oblique grid.

Fig. 5.6. Finest grids supersonic flat plate flow.

The corresponding inviscid surface pressure distributions as obtained by Osher's scheme, and with the first-order, the non-limited $\kappa = 1/3$ and the limited $\kappa = 1/3$ approximation are given in Fig. 5.7. The poor solution quality on the rectangular grid is clear. (For details about boundary conditions used and so on, we refer to [10].)

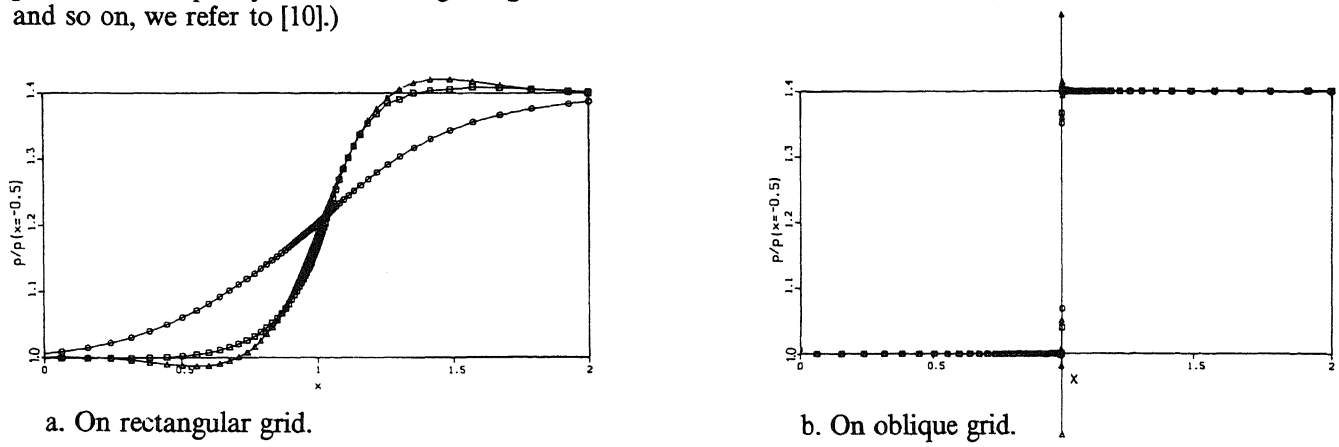

a. On rectangular grid. b. On oblique grid.

Fig. 5.7. Inviscid surface pressure distributions supersonic flat plate flow
(○ : first-order, △ : non-limited higher-order, □ : limited higher-order).

Together with the measured data, the computed viscous surface pressure distributions are given in Fig. 5.8. First we consider the results obtained on the rectangular grid. Given the bad inviscid solutions, obtained on the regular grid, it should be noticed that the good resemblance of the experimental and the second-order accurate viscous surface pressure distribution is absolutely fake. Since for this standard test case most authors use rectangular grids, and since most codes smear out discontinuities which are not aligned with the grid, a lot of good resemblance ever found for this test case might in fact be deceptive. Considering the results obtained on the oblique grid and comparing at first the computed surface pressure distributions, we see that diffusion has done its job in qualitatively different ways. In downstream direction, the second-order pressure distribution in the interaction region shows successively: a compression, a plateau and another compression. The computed second-order accurate surface pressure distribution is characteristic for a shock wave - boundary layer interaction with separation bubble (i.e. with separation and re-attachment), whereas the first-order distribution typically is the distribution belonging to a non-separating flow. Given the occurrence of a separation bubble in the experimental results indeed, the first-order solution (on this 80×32-grid) has to be rejected. Comparing the second-order and measured surface pressure distribution, it appears that the latter is more strongly diffused. An explanation for this quantitative difference is lacking. Due to all kinds of uncertainties a detailed quantitative comparison is probably impossible. Uncertain in the experiment are for instance: cross flow influences (3D effects), non-observed though influential turbulence, some slight heat transfer through the wall, and so on. Uncertainties in the computation are for instance: a possibly too crude boundary condition treatment somewhere, the neglect of temperature dependence in the diffusion coefficients, and so on.

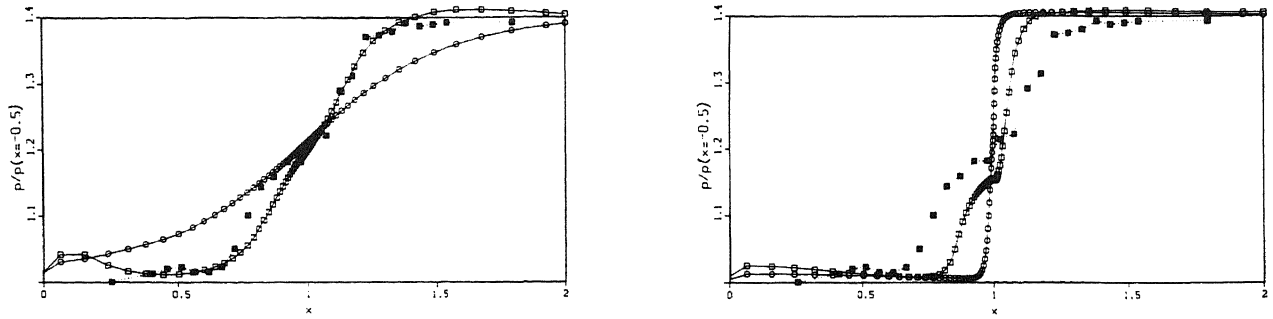

a. On rectangular grid. b. On oblique grid.

Fig. 5.8. Viscous surface pressure distributions supersonic flat plate flow
(○ : first-order, □ : limited second-order, ■ : measured).

In Fig. 5.9 some measured and computed velocity profiles are given. Once more, the figures clearly show the good quality of the second-order results. Remarkable for both the first- and second-order velocity profiles is the good agreement with the experimental data in the upper part of the boundary layer at $x = 3.62\,10^5/Re$. Both solutions seem to give a correct prediction of the growth of the boundary layer thickness through the interaction region.

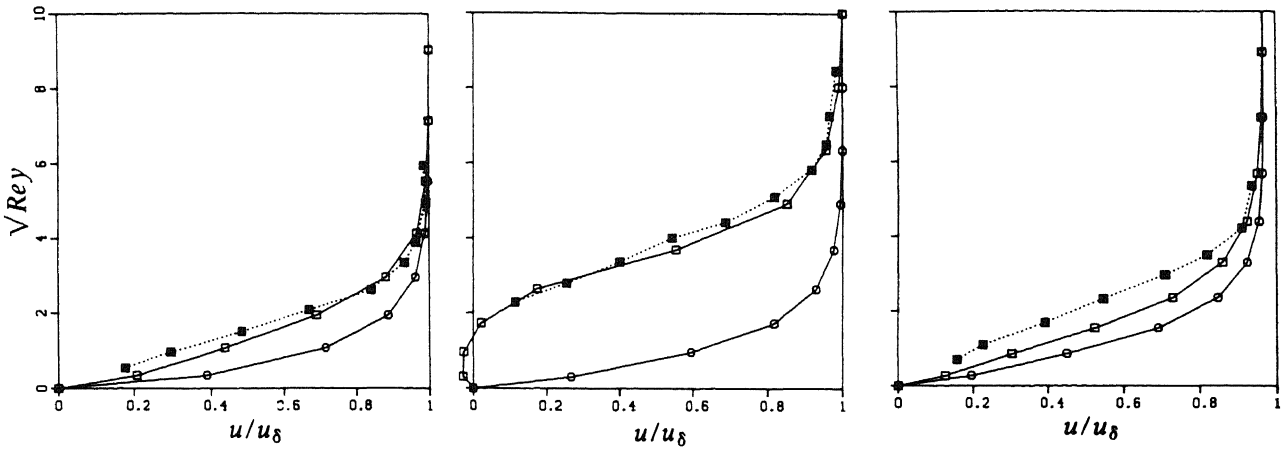

a. $x = 2.27\ 10^5/Re$ b. $x = 2.87\ 10^5/Re$ c. $x = 3.62\ 10^5/Re$

Fig. 5.9. Velocity profiles supersonic flat plate flow
(○ : first-order, □ : limited second-order, ■ : measured).

To obtain the second-order accurate solution we had to use: $\omega = 0.5$ in (4.1). Despite of the damping used, the computation is still quite efficient. For a detailed account of convergence rates and computing times we refer to [10].

6. Conclusion

To our opinion, an important practical result of the present paper is the illustrated importance of carefully checking the reliability of a computed Navier-Stokes solution. In particular, the reliability should be checked with respect to the numerical errors introduced by the discretization of the convective part. *This seems a trivial remark, but it appears that one is not sufficiently aware of this problem in practice.* For a viscous hypersonic flow computation around a winged reentry vehicle, with several severe shock wave - boundary layer interactions, such a check might be of paramount importance.

The present approach allows an easy check of false diffusion: the same code can be used both for viscous ($1/Re > 0$) and inviscid ($1/Re = 0$) flow computations.

7. PRESENT AND FUTURE RESEARCH

At the moment the existing (perfect gas) Euler code is extended to hypersonics. This seems to be possible without (much) loss of efficiency. However, it appears that the solution of hypersonic flows requires a special treatment near stagnation points. A report is in preparation [5].

The Navier-Stokes research seems worth to be continued. A next development will be the introduction of adaptive grid refinement. Further, a convergence rate improvement by the choice of another basic relaxation scheme still seems to be possible.

ACKNOWLEDGEMENT

The authors want to thank P.Wesseling, B.van Leer and C. Nebbeling for their useful advices.

REFERENCES

1. S.R. CHAKRAVARTHY, K.Y. SZEMA, U.C. GOLDBERG, J.J. GORSKI and S. OSHER (1985). *Application of a New Class of High Accuracy TVD Schemes to the Navier-Stokes Equations.* AIAA-paper 85-0165.
2. W. HACKBUSCH (1985). *Multigrid Methods and Applications.* Springer, Berlin.
3. R.J. HAKKINEN, I. GREBER, L. TRILLING and S.S. ABARBANEL (1958). *The Interaction of an Oblique Shock Wave with a Laminar Boundary Layer.* NASA-memorandum 2-18-59 W.
4. P.W. HEMKER (1986). *Defect Correction and Higher Order Schemes for the Multi Grid Solution of the Steady Euler Equations.* Proceedings of the 2nd European Conference on Multigrid Methods, Cologne 1985, Springer, Berlin.
5. ------ and B. KOREN (1988). *Pilot Computations of Hypersonic Equilibrium Flows with an Existing Steady Euler Code.* CWI Report NM-R88xx, Amsterdam (to appear).
6. ------ and S.P. SPEKREIJSE (1986). *Multiple Grid and Osher's Scheme for the Efficient Solution of the Steady Euler Equations.* Appl. Num. Math. 2, 475-493.
7. B. KOREN (1987). *Euler Flow Solutions for a Transonic Wind Tunnel Section.* Proceedings V-Aerodynamic Seminar, Aachen, 1987 (to appear).
8. ------ (1988). *Defect Correction and Multigrid for an Efficient and Accurate Computation of Airfoil Flows.* J. Comput. Phys. (to appear).
9. ------ (1988). *First-Order Upwind Schemes and Multigrid for the Steady Navier-Stokes Equations.* CWI report NM-R88yy, Amsterdam (to appear).
10. ------ (1988). *Higher-Order Upwind Schemes and Defect Correction for the Steady Navier-Stokes Equations.* CWI report NM-R88zz, Amsterdam (to appear).
11. ------ and S.P. SPEKREIJSE (1987). *Multigrid and Defect Correction for the Efficient Solution of the Steady Euler Equations.* Proceedings of the 25th Meeting of the Dutch Association for Numerical Fluid Mechanics, Delft, 1986. Notes on Numerical Fluid Mechanics 17, Vieweg, Braunschweig.
12. B. VAN LEER (1982). *Flux-Vector Splitting for the Euler Equations.* Proceedings of the 8th International Conference on Numerical Methods in Fluid Dynamics, Aachen, 1982. Lecture Notes in Physics 170, Springer, Berlin.
13. ------ (1985). *Upwind-Difference Methods for Aerodynamic Problems governed by the Euler Equations.* Proceedings of the 15th AMS-SIAM Summer Seminar on Applied Mathematics, Scripps Institution of Oceanography, 1983. Lectures in Applied Mathematics 22, AMS, Providence, Rhode Island.
14. S. OSHER and F. SOLOMON (1982). *Upwind-Difference Schemes for Hyperbolic Systems of Conservation Laws.* Math. Comp. 38, 339-374.
15. R. PEYRET and T.D. TAYLOR (1983). Computational Methods for Fluid Flow. Springer, Berlin.
16. W. SCHRÖDER and D. HÄNEL (1987). *An Unfactored Implicit Scheme with Multigrid Acceleration for the Solution of the Navier-Stokes Equations.* Computers and Fluids 15, 313-336.
17. G. SHAW and P. WESSELING (1986). *Multigrid Solution of the Compressible Navier-Stokes Equations on a Vector Computer.* Proceedings of the 10th International Conference on Numerical Methods in Fluid Dynamics, Beijing, 1986. Lecture Notes in Physics 264, Springer, Berlin.
18. S.P. SPEKREIJSE (1987). *Multigrid Solution of Monotone Second-Order Discretizations of Hyperbolic Conservations Laws.* Math. Comp. 49, 135-155.
19. ------ (1987). *Multigrid Solution of the Steady Euler Equations.* Ph.D.-thesis, CWI, Amsterdam.
20. J.L. THOMAS and R.W. WALTERS (1985). *Upwind Relaxation Algorithms for the Navier-Stokes Equations.* AIAA-paper, 86-1501.